

Photophysics of Intrinsic Single-Photon Emitters in Silicon Nitride at Low Temperatures

Zachariah O. Martin, Alexander Senichev, Samuel Peana, Benjamin J. Lawrie, Alexei S. Lagutchev, Alexandra Boltasseva, and Vladimir M. Shalaev*

A robust process for fabricating intrinsic single-photon emitters in silicon nitride is recently established. These emitters show promise for quantum applications due to room-temperature operation and monolithic integration with technologically mature silicon nitride photonics platforms. Here, the fundamental photophysical properties of these emitters are probed through measurements of optical transition wavelengths, linewidths, and photon antibunching as a function of temperature from 4.2 to 300 K. Important insight into the potential for lifetime-limited linewidths is provided through measurements of inhomogeneous and temperature-dependent broadening of the zero-phonon lines. At 4.2 K, spectral diffusion is found to be the main broadening mechanism, while spectroscopy time series reveal zero-phonon lines with instrument-limited linewidths.

sensing, and quantum memories.^[1–7] Heralded single-photon sources utilizing nonlinear processes such as spontaneous parametric down-conversion or four-wave mixing can produce single-photons with near-unity indistinguishability and have been used for ground-breaking demonstrations of satellite-based quantum communication^[8,9] and quantum computational advantage.^[10,11] One of the drawbacks of the demonstrated heralded nonlinear sources is the probabilistic nature of single-photon generation, which results in substantial obstacles to scalable quantum technologies.^[12,13] In contrast, single photon emission from localized excitons or color centers in solids can be deterministic with sufficient control of the excitation and

1. Introduction

Single-photon sources form a critical building block for quantum information technologies such as all-optical quantum computing schemes, quantum communication protocols, quantum

collection efficiency.^[7,14] Much research attention has been given to the search for solid-state single photon emitters (SPEs) that can emit indistinguishable photons on demand into desired optical modes. The nitrogen-vacancy and silicon-vacancy centers in diamond, single quantum dots, and the various color centers in hexagonal boron nitride (hBN) have been rapidly developed in recent years for this purpose.^[1,3,5–7,15–18] Moreover, these solid-state SPEs promise integrability with large-scale on-chip quantum photonic circuitry.

Researchers have made substantial advances in hybrid integration approaches, where an emitter in one material couples to a photonic element made of another material.^[7,19,20] Since some materials that host SPEs cannot readily serve as photonic elements – due to intrinsic losses, difficulties in growing wafer-scale films, or nanofabrication challenges – these approaches enabled the on-chip integration of solid-state SPEs with favorable optical properties.^[7,19,20] Drawbacks of hybrid integration, however, include increased device fabrication complexity and coupling losses at the interface between the SPE host material and the photonic element. Consequently, growing research efforts have targeted new species of color centers in materials that can also serve as a photonic platform. This monolithic integration approach avoids the fabrication complexity and coupling losses of hybrid integration schemes. Promising results with new defect species in photonic materials include that of the carbon-based G-center and other emitters in silicon (Si),^[21–23] color centers in gallium nitride (GaN),^[24] color centers in aluminum nitride,^[25–28] and the various defect centers in silicon carbide (SiC).^[29–37] In addition to having outstanding optical properties, these defects have been monolithically integrated into photonic

Z. O. Martin, A. Senichev, S. Peana, A. S. Lagutchev, A. Boltasseva, V. M. Shalaev
Elmore Family School of Electrical and Computer Engineering, Birck Nanotechnology Center and Purdue Quantum Science and Engineering Institute
Purdue University
610 Purdue Mall, West Lafayette, IN 47907, USA
E-mail: shalaev@purdue.edu

Z. O. Martin, A. Senichev, S. Peana, B. J. Lawrie, A. S. Lagutchev, A. Boltasseva, V. M. Shalaev
Quantum Science Center, Department of Energy, A National Quantum Information Science Research Center of the U.S
Oak Ridge National Laboratory
1 Bethel Valley Road, Oak Ridge, TN 37830, USA

B. J. Lawrie
Materials Science and Technology Division
Oak Ridge National Laboratory
1 Bethel Valley Road, Oak Ridge, TN 37830, USA

 The ORCID identification number(s) for the author(s) of this article can be found under <https://doi.org/10.1002/qute.202300099>

© 2023 The Authors. Advanced Quantum Technologies published by Wiley-VCH GmbH. This is an open access article under the terms of the Creative Commons Attribution-NonCommercial-NoDerivs License, which permits use and distribution in any medium, provided the original work is properly cited, the use is non-commercial and no modifications or adaptations are made.

DOI: 10.1002/qute.202300099

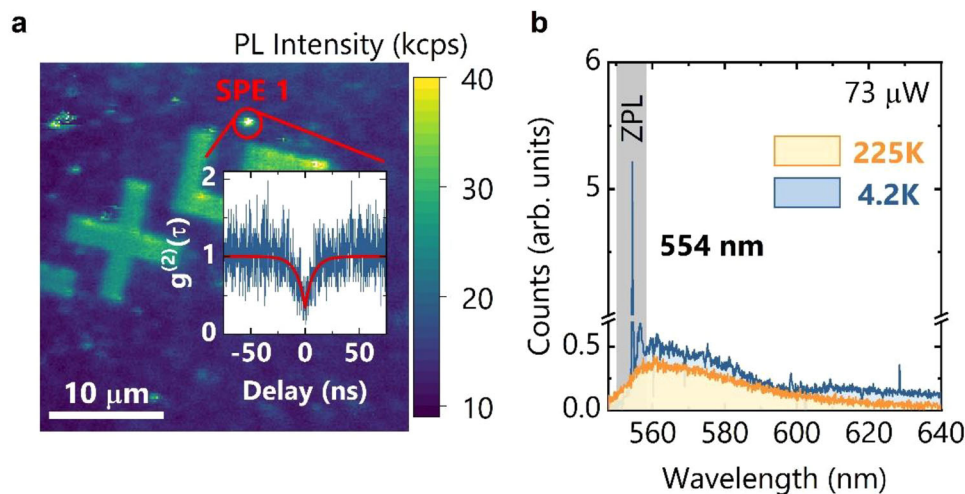


Figure 1. Characterization of a representative SPE in SiN at cryogenic temperature. a) PL intensity map of a SiN sample containing SPEs. The red circle indicates the position of the representative emitter characterized in (b). The inset shows the emitter's second-order autocorrelation histogram, with an antibunching value of $g^{(2)}(0) = 0.41 \pm 0.04$. b) Background-corrected room temperature (red) and $T = 4.2$ K (blue) spectra of the representative SPE with the ZPL highlighted in the low-temperature spectrum.

structures such as waveguides or 1D photonic crystals with high coupling efficiency.^[21,22,26,29,30,35,36,38–40]

We have recently discovered a new type of SPE in silicon nitride (SiN) films, which exhibits high single-photon purity at room temperature and promises seamless integration with a technologically mature material platform.^[41] These intrinsic SiN quantum emitters are stable, bright, and linearly polarized, which makes them exciting candidates for quantum photonic applications.^[41] Furthermore, this development is of particular technological interest due to the low losses in SiN and mature fabrication techniques established for SiN photonic circuit elements.^[42,43] SiN has become a leading material platform for quantum photonic computing and is employed by industry leaders and emerging photonic companies such as Xanadu and QuiX Quantum.^[11,44,45] We have also demonstrated the monolithic integration of SiN color centers into waveguides and the deterministic placement of emitters with patterned nanopillar arrays.^[46,47]

At room temperature, SiN SPEs produce a broad photoluminescence (PL) spectrum that consists of multiple overlapping bands. For most SiN SPEs, these bands cluster around specific wavelengths, but at room temperature, the PL spectrum lacks a distinct zero phonon line (ZPL) peak, and the nature of the optical transitions responsible for the broad spectral components has been unclear until now.^[41] Moreover, as we have previously shown, understanding and controlling additional spectral lines in SPEs is critical to their ultimate use in quantum technologies.^[48,49] Here, we study the optical transition wavelengths, linewidths, and photon antibunching properties of these emitters as a function of temperature from 4 to 300 K. At cryogenic temperatures, we find the emergence of narrow emission lines on top of the broad spectrum, which allows us to identify the distribution of SiN SPE ZPLs. We also find that spectral diffusion is the dominant broadening mechanism at 4.2 K. Time series of PL spectra further allow us to resolve ZPL peaks whose average linewidth of 71.5 ± 27.7 GHz is limited by the spectrometer resolution.

2. Results and Discussion

Following the emitter creation procedure established previously,^[41] we fabricated SiN films that contain intrinsic single photon emitters. PL intensity maps acquired at $T = 4.2$ K reveal the presence of isolated bright spots, which were confirmed to be single photon emitters by second-order autocorrelation measurements (inset of **Figure 1a**). We then compare 4.2 K and room-temperature PL spectra from SPEs in these SiN films that have been background corrected to emphasize the contribution from the emitters themselves (**Figure 1b**). As the sample is cooled below 200 K, a sharp peak clearly appears on top of these broad peaks ≈ 554 nm, which we assign to the ZPL (**Figure 1b**, blue).

The PL spectra observed at room temperature from isolated emitters are consistent with our previous report^[41] and are comprised of broad peaks spanning the visible range (**Figure 2a,b**, yellow). These broad spectral features—which we tentatively assign to phonon sidebands (PSBs)—fit well to Gaussian peaks centered at ≈ 567 , 596, 632, and 670 nm (**Figure 2a,b**, yellow).^[41] We then collect additional statistics on the ZPL energy measured at 4.2 K for 17 ZPLs and find an average emission wavelength of 548 nm with a standard deviation of ≈ 7 nm (**Figure 2c**). Thus, we conclude that the lack of a clear ZPL transition in the previously reported SPE spectra^[41] is a result of a large Huang–Rhys factor that leads to strong PSBs relative to the ZPL at room temperature. A 550 nm longpass filter that was used to acquire the previously reported spectra also minimized the appearance of the ZPL.

At low temperatures, along with the ZPL transitions ≈ 548 nm, additional redshifted sharp peaks consistently emerge atop the PSBs (**Figure 2b**, blue). These additional sharp lines also observed could originate from other nearby emitters or unidentified transitions, the origin of which will be discussed in detail below.

We also note that ZPL wavelengths from SPEs in SiN tend to cluster around the Si Raman line at 547.2 nm (520 cm^{-1}) under 532 nm excitation. The ZPL emission is clearly distinct from the

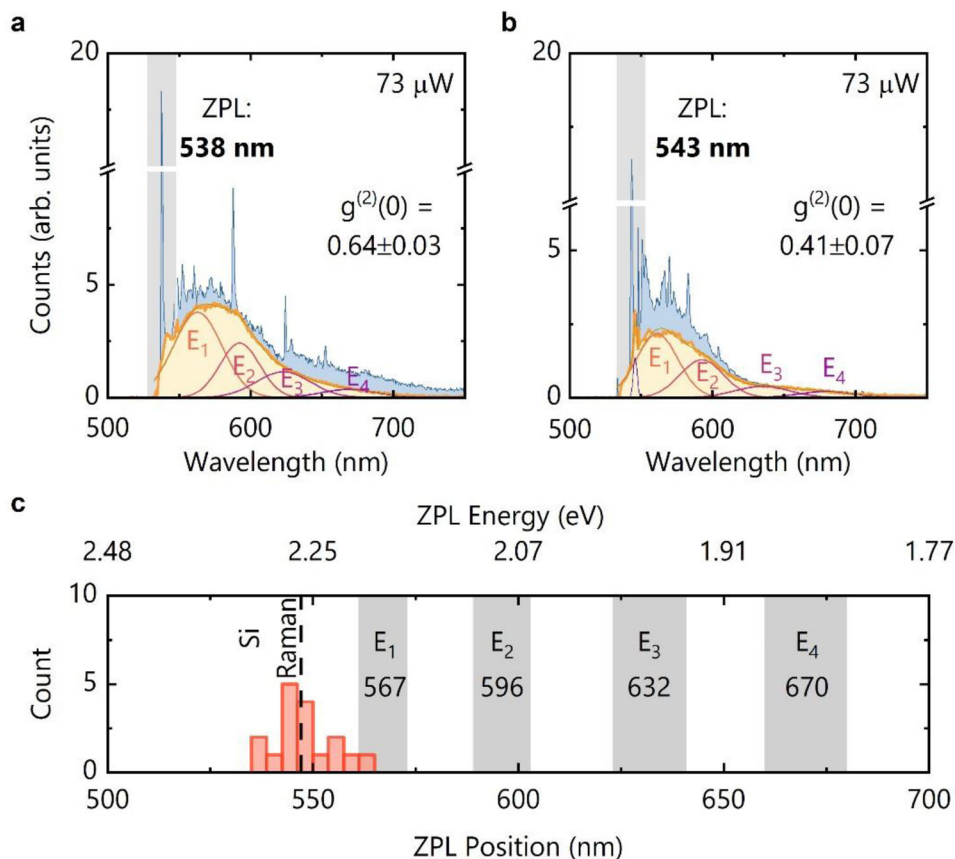


Figure 2. a,b) Background-corrected PL spectra taken from representative emitters at 4.2 K (blue) and room temperature (yellow). The 4.2 K and room-temperature PL intensities are scaled for comparison. c) Histogram of ZPL peak position acquired from 17 emitters. Shaded regions labeled E_1 , E_2 , E_3 , and E_4 indicate the position of broad peaks typically resolved in room temperature spectra.^[41]

Si Raman line though, as it only appears at the positions of localized emitters whereas the Si Raman peak is a feature of the underlying Si substrate and is present everywhere (see Figures S1 and S2, Supporting Information). Further, the ZPL emission wavelength and linewidth show clear temperature dependence, as will be discussed below, but the Si Raman line position and linewidth do not change in the temperature range of 4.2–300 K (see Figure S3, Supporting Information).

Note that we observed somewhat reduced SPE purity at low temperatures, which we attribute to a larger beam spot size used for low-temperature PL measurements as well as leakage of the 2TO Si Raman and a lower ratio of emission into the PSBs. We find a median $g^{(2)}(0)$ value of 0.43 at low temperatures and a median $g^{(2)}(0)$ value of 0.11 at room temperature from the same sample. More discussion of the $g^{(2)}(0)$ distribution is presented in Section S2 (Supporting Information).

Understanding and controlling the dephasing processes in SPEs and demonstrating transform-limited transitions with near-unity photon indistinguishability is critical to the development of quantum photonic technologies. Thus, we measured consecutive PL spectra of a ZPL at ≈ 562 nm center wavelength at high spectral resolution every 5.0 s to capture inhomogeneous broadening mechanisms and to probe the fundamental limits of these intrinsic SPEs at 4.2 K. The time-integrated spectrum shown in Figure 3a can be well fitted by a Voigt peak with a

linewidth of 266 GHz, with a Gaussian component of 219 GHz and a Lorentzian component of 76 GHz. Clearly, the ZPL is dominated by the Gaussian component of the peak, which indicates that inhomogeneous broadening is the main broadening mechanism at 4.2 K. The dominance of spectral diffusion is also evident from the time trace of PL spectra (bottom of Figure 3a) as the ZPL peak position wanders erratically over the course of the measurement. This spectral wandering is also present in time traces of PL spectra taken from other emitters (see Section S3, Supporting Information). The 2nd-order transverse optical (2TO) Si Raman mode appears in the spectrum time series since it is not background-corrected (labeled at the top of Figure 3a). However, analysis of a single frame that was integrated for 5 s (Figure 3b) reveals the presence of multiple, narrower ZPL peaks. These narrow peaks fit well to Lorentzian functions and have linewidths of 90, 55, and 30 GHz. From fitting all ZPL peaks resolved in the 30 frames of Figure 3a, we find an average ZPL linewidth of 71.5 ± 27.7 GHz – which is just over twice the resolution limit of 27.2 GHz (Figure 3c) and consistent with fitting the integrated spectrum. We also find that the rate and range of spectral wandering decrease at lower excitation power, which could potentially be used to control spectral diffusion (see Section S4, Supporting Information).

Finally, we measure PL spectra and extract peak positions and linewidths over a range of temperatures from 4.2 to 300 K.

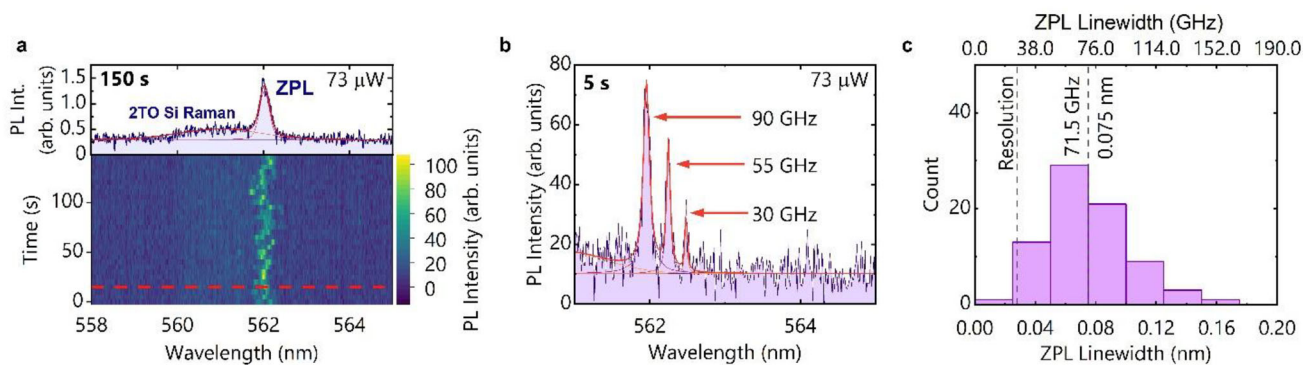


Figure 3. a) Time series of PL spectra from another emitter taken at 4.2 K using 0.029 nm resolution. The top plot shows the time-integrated (integrated for 150 s) spectrum. b) An individual frame of the spectrum time series (integrated for 5 s) indicated by the dashed red line in (a). c) Histogram of ZPL FWHM values extracted from fitting 30 5.0 s integrated PL spectra. Dashed lines indicate the spectrometer resolution limit (27.2 GHz or 0.028 nm) and the average ZPL linewidth (71.5 ± 27.7 GHz or 0.075 ± 0.028 nm). The bin size is 24 GHz (0.025 nm).

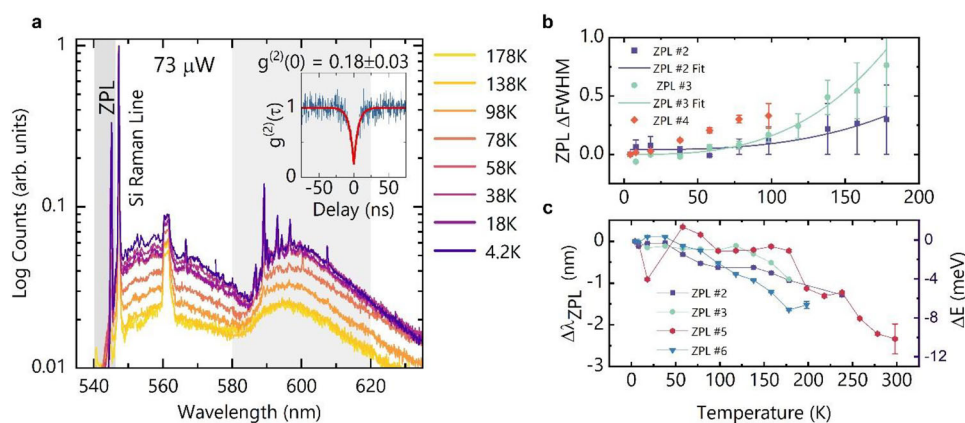


Figure 4. Temperature-dependent PL spectra analysis. a) Gradual emergence of narrow linewidth peaks in the SPE's PL spectrum with decreasing temperature (log scale, without background correction). Inset: second-order autocorrelation histogram recorded at 4.2 K confirming the single-photon nature of the emitter. A shaded region indicates a spectral range where additional sharp peaks tend to occur. b) Increase in the ZPL linewidth with increasing temperature from fitting temperature-dependent spectra of additional emitters. c) Change in ZPL energy of selected emitters from 4.2 to 300 K.

As the temperature decreases, the broad emission peaks seen at room temperature are preserved, and sharp emission lines gradually begin to emerge on top of them (Figure 4a; note that spectra are not background corrected and a logarithmic scale is used). The additional redshifted sharp peaks mentioned earlier emerge between 580 and 620 nm (shaded gray region in Figure 4a). Additionally, Figure 4b,c reveals the temperature-dependent ZPL broadening and energy shift from fitting spectra taken from several different emitters (photophysical properties of selected representative emitters are listed in Table S1, Supporting Information). In some cases, the increase in ZPL linewidth can be well fitted with a T^3 dependence, which is similar to the behavior of other solid-state emitters reported in the literature and consistent with the scaling typically seen in phonon-induced broadening.^[27,50] The linewidth reaches 1.45 THz at ≈ 200 K, which is comparable to the linewidth observed at room temperature from other solid-state SPEs such as color centers in hBN^[51] and diamond.^[52] The ZPL peak position exhibits an overall redshift with increasing temperature, however, the ZPL energies of some emitters behave quite nonmonotonically as a

function of temperature from ≈ 4 to ≈ 150 K (Figure 4c). This “S-shaped” or anomalous temperature dependence is also observed in GaN SPEs^[53] and core-shell quantum dots.^[54] This trend was attributed to carrier reshuffling within stacking faults in GaN,^[53] and temperature-dependent optical phonon coupling in quantum dots.^[54] The fact that a similar effect is seen in SiN SPEs also suggests a more complicated defect structure than a simple atomic defect or rich materials physics at the interface between SiN and silicon dioxide (SiO₂) formed after annealing.

As discussed previously, the low-temperature PL spectra of SiN SPEs consist of a ZPL, PSBs, and additional peaks (shaded gray regions in Figures 4a and 5a) which may originate from nearby SiN emitters or other unidentified transitions. We present low-temperature spectra from another representative SPE (Figure 5a) to highlight this finding. In addition to the ZPL, we label the three additional peaks near 600 nm as V_1 , V_2 , and V_3 . These three modes appear consistently in the 580–620 nm wavelength band in low-temperature PL spectra taken from several emitters, with an average ZPL- V_1 separation of 170 meV and average $V_1/V_2/V_3$ -peak separation of roughly 10 meV (Figure 5b). Similar spectral

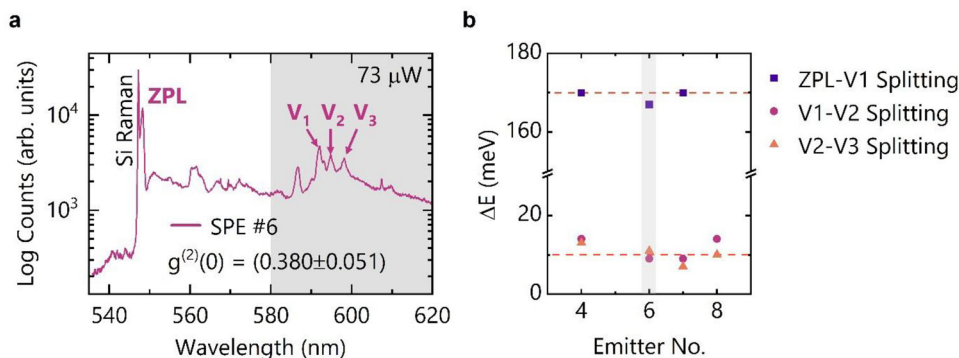


Figure 5. a) 4.2 K spectrum of a representative emitter highlighting the presence of a ZPL and redshifted sharp peaks, with three peaks that we identify as vibronic modes labeled as V_1 , V_2 , and V_3 . The spectral range where additional sharp peaks appear is shaded gray. b) Comparison of the energy splitting between the ZPL and vibronic peaks for several representative ZPLs, as well as the energy differences between the vibronic peaks. The emitter whose spectra are shown in part (a) is highlighted.

features have been previously observed in low-temperature spectra of both single organic molecules^[55] and optically active defects formed at the interface of SiC and SiO₂.^[56] In the case of single organic molecules, sharp lines that are red-shifted from the ZPL also sit atop a broad peak; these lines correspond to localized vibronic modes of the crystal that the electronic transition couples to. The splitting between vibronic peaks of 5–10 meV observed in single dibenzoterrylene molecules is also similar to what we observe here.^[55] At 4.2 K, SiC/SiO₂-related defects exhibit a pronounced ZPL with a group of additional red-shifted narrow lines, which were assigned to various components of the vibronic sidebands. Due to the defects' proximity to the interface, it was argued that these sidebands consist of both SiC and SiO₂ intrinsic phonons.^[56] The splitting between the ZPL and the vibronic sidebands was also found to be between 150 and 220 meV, which is similar to the splitting observed in our work on the SiN/SiO₂ system.^[56] Therefore, we hypothesize that the additional sharp peaks observed in low-temperature SiN SPE spectra with consistent energy spacing from the ZPL could originate from vibronic modes.

The findings of our work further corroborate that the observed SPEs in SiN are related to a single defect family. The rich structure of the vibronic modes indicates that the defect structure could be more complex than defects existing within Si–Si or N–N bonds and may also include oxygen from the SiO₂ interface. It is also possible that partial crystallization of the SiN layer at the SiO₂ interface which occurs during annealing contributes to the presence of these vibronic modes.^[57–59]

3. Conclusion

The narrow-linewidth spectral content that emerges in SiN SPE PL spectra at low temperatures provides an important foundation to gain insights into 1) the atomistic origin of these emitters; 2) spectral diffusion effects that cannot be resolved at higher temperatures due to a large Huang–Rhys factor, and 3) the means to control the SPE linewidth to achieve the sought-after high-indistinguishability SPEs in a technologically mature material platform. At 4.2 K, we showed that the ZPL linewidth is predominantly determined by the spectral diffusion with narrow peaks whose linewidths are limited by the spectrometer reso-

lution. Though inhomogeneous broadening remains a hurdle, there is a potential to obtain lifetime-limited emission at low temperatures for quantum photonic applications. We previously reported an average SiN SPE excited state lifetime of 2.4 ns, so the expected transform-limited linewidth is ≈ 70 MHz. Moving forward, photoluminescence excitation spectroscopy and Hong–Ou–Mandel interferometry are needed to corroborate the intrinsic linewidth and potential photon indistinguishability, respectively. Electrostatic control^[60] and strain tuning^[61,62] have recently been used to suppress spectral diffusion for emitters in hBN and diamond, and a similar reduction in inhomogeneous broadening could be achieved with functionalization of the proposed SPE platform guided by appropriate theoretical modeling. This would pave the way to future quantum photonic circuitry with elements containing monolithically integrated, actively controlled SPEs.

4. Experimental Section

PL Setup: Room temperature optical characterization was performed using a custom-made scanning confocal microscope with a 100 μm pinhole based on a commercial inverted microscope body (Nikon Ti–U). To perform PL intensity mapping, a P-561 piezo stage driven by an E-712 controller (Physik Instrumente) scanned a 100x air objective with a 0.95 numerical aperture (NA). A continuous wave 532 nm laser (RGB Photonics) was used for excitation. The excitation beam was reflected off a 550 nm long-pass dichroic mirror (DMLP550L, Thorlabs), and a 550 nm long-pass filter (FEL0550, Thorlabs) was used to filter out the remaining pump power. Two avalanche detectors with a 30 ps time resolution and 35% quantum efficiency at 650 nm (PDM, Micro-Photon Devices) were used for single-photon autocorrelation measurements. Time-correlated photon counting was performed by a correlation card “start-stop” acquisition card with a 4 ps internal jitter (SPC-150, Becker & Hickl).

Low-temperature PL characterization of emitters was performed using a home-built confocal PL microscope integrated into a closed-cycle Montana S100 cryostation. A Princeton Instruments Isoplanar SCT-320 spectrograph with a Pixis 400BR Excelon camera was used to measure PL spectra. A grating with 2400 grooves/mm was used to measure ZPLs in Figure 3 with a spectral resolution of 0.029 nm, and a grating with 600 grooves/mm was used to measure the broader spectra in Figures 2, 4, and 5 with a spectral resolution of 0.13 nm. For a direct comparison of room temperature and low-temperature spectra over most of the visible range in Figure 1, a grating with 150 grooves/mm and a spectral resolution of 0.55 nm was used. A 532 nm Cobolt diode laser was used to excite the SPEs via a 100x

in-vacuum objective (Zeiss, NA = 0.85). A 2-axis galvo scanner integrated with a 4f imaging system was used to acquire PL spectrum images. Photon antibunching measurements were acquired concurrently with PL spectra via a 90:10 non-polarizing beam splitter that delivered 90% of the PL to a 50:50 fiber beamsplitter and a pair of large-area superconducting nanowire single-photon detectors. A 550 nm long-pass filter was used to filter out the residual laser line for antibunching measurements. A Picoquant Hydraharp time-correlated single photon counting (TCSPC) system was used to time tag-detected photon events and calculate the histogram of photon coincidences.

Growth and Annealing: Samples containing SiN single photon emitters were prepared by a similar process to that reported previously.^[41,46] First, SiO₂ films were grown on top of commercially available Si substrates by HDPCVD (Plasma-Therm Apex SLR). The SiN layer was then grown on top of the oxide layer by the same process. As in previous reports, a nitrogen-rich growth recipe was employed to form the SiN layer. The ratio of precursors N₂ to SiH₄ was set to 1.74, producing a non-stoichiometric film with low auto-fluorescence in the visible region. The samples then underwent rapid thermal annealing (RTA) at 1100 °C for 120 s in a Jipelec Jetfirst RTA system immediately after growth to activate SPEs. This procedure could reliably produce bright, stable, linearly polarized, and high-purity SPEs in SiN films with low background autofluorescence.

Supporting Information

Supporting Information is available from the Wiley Online Library or from the author.

Acknowledgements

The cryo-optical spectroscopies described here were supported by the US Department of Energy, Office of Science, National Quantum Information Science Research Centers, Quantum Science Center. The sample preparation, material, and optical characterization were supported by National Science Foundation (NSF) grant 2015025-ECCS and Purdue's Elmore ECE Emerging Frontiers Center "The Crossroads of Quantum and AI." Low-temperature photoluminescence measurements were conducted as part of a user project at the Center for Nanophase Materials Sciences (CNMS), which is a US Department of Energy, Office of Science User Facility at Oak Ridge National Laboratory.

Conflict of Interest

No. The authors declare no conflict of interest.

Data Availability Statement

The data that support the findings of this study are available from the corresponding author upon reasonable request.

Keywords

photophysics, quantum photonics, silicon nitride, single-photon emitters

Received: May 3, 2023
Revised: August 3, 2023
Published online:

[1] C. Bradac, W. Gao, J. Forneris, M. E. Trusheim, I. Aharonovich, *Nat. Commun.* **2019**, *10*, 5625.

- [2] B. J. M. Hausmann, B. Shields, Q. Quan, P. Maletinsky, M. McCutcheon, J. T. Choy, T. M. Babinec, A. Kubanek, A. Yacoby, M. D. Lukin, M. Lončar, *Nano Lett.* **2012**, *12*, 1578.
- [3] T. Schröder, S. L. Mouradian, J. Zheng, M. E. Trusheim, M. Walsh, E. H. Chen, L. Li, I. Bayn, D. Englund, *J. Opt. Soc. Am. B* **2016**, *33*, B65.
- [4] C. T. Nguyen, D. D. Sukachev, M. K. Bhaskar, B. MacHielse, D. S. Levonian, E. N. Knall, P. Stroganov, R. Riedinger, H. Park, M. Lončar, M. D. Lukin, *Phys. Rev. Lett.* **2019**, *123*, 1.
- [5] I. Aharonovich, S. Castelletto, D. A. Simpson, C. H. Su, A. D. Greentree, S. Praver, *Rep. Prog. Phys.* **2011**, *74*, 076501.
- [6] A. Gottscholl, M. Kianinia, V. Soltamov, S. Orlinskii, G. Mamin, C. Bradac, C. Kasper, K. Krambrock, A. Sperlach, M. Toth, I. Aharonovich, V. Dyakonov, *Nat. Mater.* **2020**, *19*, 540.
- [7] I. Aharonovich, D. Englund, M. Toth, *Nat. Photonics* **2016**, *10*, 631.
- [8] S. K. Liao, W. Q. Cai, W. Y. Liu, L. Zhang, Y. Li, J. G. Ren, J. Yin, Q. Shen, Y. Cao, Z. P. Li, F. Z. Li, X. W. Chen, L. H. Sun, J. J. Jia, J. C. Wu, X. J. Jiang, J. F. Wang, Y. M. Huang, Q. Wang, Y. L. Zhou, L. Deng, T. Xi, L. Ma, T. Hu, Q. Zhang, Y. A. Chen, N. le Liu, X. bin Wang, Z. C. Zhu, C. Y. Lu, et al., *Nature* **2017**, *549*, 43.
- [9] Y. A. Chen, Q. Zhang, T. Y. Chen, W. Q. Cai, S. K. Liao, J. Zhang, K. Chen, J. Yin, J. G. Ren, Z. Chen, S. L. Han, Q. Yu, K. Liang, F. Zhou, X. Yuan, M. S. Zhao, T. Y. Wang, X. Jiang, L. Zhang, W. Y. Liu, Y. Li, Q. Shen, Y. Cao, C. Y. Lu, R. Shu, J. Y. Wang, L. Li, N. le Liu, F. Xu, X. bin Wang, et al., *Nature* **2021**, *589*, 214.
- [10] H.-S. Zhong, H. Wang, Y.-H. Deng, M.-C. Chen, L.-C. Peng, Y.-H. Luo, J. Qin, D. Wu, X. Ding, Y. Hu, P. Hu, X.-Y. Yang, W.-J. Zhang, H. Li, Y. Li, X. Jiang, L. Gan, G. Yang, L. You, Z. Wang, L. Li, N.-L. Liu, C.-Y. Lu, J.-W. Pan, *Science* **2020**, *370*, 1460.
- [11] L. S. Madsen, F. Laudenbach, M. F. Askarani, F. Rortais, T. Vincent, J. F. F. Bulmer, F. M. Miatto, L. Neuhaus, L. G. Helt, M. J. Collins, A. E. Lita, T. Gerrits, S. W. Nam, V. D. Vaidya, M. Menotti, I. Dhand, Z. Vernon, N. Quesada, J. Lavoie, *Nature* **2022**, *606*, 75.
- [12] S. Signorini, L. Pavesi, *AVS Quantum Sci.* **2020**, *2*, 0018594.
- [13] E. Meyer-Scott, C. Silberhorn, A. Migdall, *Rev. Sci. Instrum.* **2020**, *91*, 041101.
- [14] G. Moody, V. J. Sorger, D. J. Blumenthal, P. W. Juodawlkis, W. Loh, C. Sorace-agaskar, A. E. Jones, K. C. Balram, J. C. F. Matthews, A. Laing, M. Davanco, L. Chang, J. E. Bowers, N. Quack, C. Galland, I. Aharonovich, M. A. Wolff, C. Schuck, N. Sinclair, M. Lon, T. Komljenovic, D. Weld, S. Mookherjee, S. Buckley, M. Radulaski, S. Reitzenstein, B. Pingault, B. Machielse, D. Mukhopadhyay, *J. Phys. Photonics* **2022**, *4*, 1.
- [15] K. Nemoto, M. Trupke, S. J. Devitt, B. Scharfenberger, K. Buczak, J. Schmiedmayer, W. J. Munro, *Sci. Rep.* **2016**, *6*, 26284.
- [16] M. Pompili, S. L. N. Hermans, S. Baier, H. K. C. Beukers, P. C. Humphreys, R. N. Schouten, R. F. L. Vermeulen, M. J. Tiggelman, L. dos Santos Martins, B. Dirkse, S. Wehner, R. Hanson, *Science* **2021**, *372*, 259.
- [17] T. T. Tran, C. Elbadawi, D. Totonjian, C. J. Lobo, G. Grosso, H. Moon, D. R. Englund, M. J. Ford, I. Aharonovich, M. Toth, *ACS Nano* **2016**, *7*, 331.
- [18] R. Uppu, F. T. Pedersen, Y. Wang, C. T. Olesen, C. Papon, X. Zhou, L. Midolo, S. Scholz, A. D. Wieck, A. Ludwig, P. Lodahl, *Sci. Adv.* **2020**, *6*, abc8268.
- [19] J.-H. Kim, S. Aghaeimeibodi, J. Carolan, D. Englund, E. Waks, *Optica* **2020**, *7*, 291.
- [20] A. W. Elshaari, W. Pernice, K. Srinivasan, O. Benson, V. Zwiller, *Nat. Photonics* **2020**, *14*, 285.
- [21] M. Prabhu, C. Errando-Herranz, L. De Santis, I. Christen, C. Chen, C. Gerlach, D. R. Englund, *Nat. Commun.* **2023**, *14*, 2380.
- [22] W. Redjem, A. Durand, T. Herzig, A. Benali, S. Pezzagna, J. Meijer, A. Y. Kuznetsov, H. S. Nguyen, S. Cuffe, J.-M. Gérard, I. Robert-Philip, B. Gil, D. Caliste, P. Pochet, M. Abbarchi, V. Jacques, A. Dréau, G. Cassabois, *Nat. Electron* **2020**, *3*, 738.

- [23] M. Hollenbach, Y. Berencén, U. Kentsch, M. Helm, G. V. Astakhov, *Opt. Express* **2020**, *28*, 26111.
- [24] A. M. Berhane, K. Y. Jeong, Z. Bodrog, S. Fiedler, T. Schröder, N. V. Triviño, T. Palacios, A. Gali, M. Toth, D. Englund, I. Aharonovich, *Adv. Mater.* **2017**, *29*, 1605092.
- [25] S. G. Bishop, J. P. Hadden, F. D. Alzahrani, R. Hekmati, D. L. Huffaker, W. W. Langbein, A. J. Bennett, *ACS Photonics* **2020**, *7*, 1636.
- [26] T. J. Lu, B. Lienhard, K. Y. Jeong, H. Moon, A. Iranmanesh, G. Grosso, D. Englund, *ACS Photonics* **2020**, *7*, 2650.
- [27] Y. Xue, H. Wang, N. Xie, Q. Yang, F. Xu, B. Shen, J. J. Shi, D. Jiang, X. Dou, T. Yu, B. Q. Sun, *J. Phys. Chem. Lett.* **2020**, *11*, 2689.
- [28] Y. Xue, T. Wei, H. Chang, D. Liang, X. Dou, B. Q. Sun, *J. Phys. Chem. C* **2021**, *125*, 11043.
- [29] S. Castelletto, *Mater. Quantum Technol.* **2021**, *1*, 023001.
- [30] A. Lohrmann, B. C. Johnson, J. C. McCallum, S. Castelletto, *Rep. Prog. Phys.* **2017**, *80*, 034502.
- [31] S. Castelletto, B. C. Johnson, V. Ivády, N. Stavrias, T. Umeda, A. Gali, T. Ohshima, *Nat. Mater.* **2014**, *13*, 151.
- [32] D. J. Christle, A. L. Falk, P. Andrich, P. V. Klimov, J. U. Hassan, N. T. Son, E. Janzén, T. Ohshima, D. D. Awschalom, *Nat. Mater.* **2015**, *14*, 160.
- [33] B. Lienhard, T. Schröder, S. Mouradian, F. Dolde, T. T. Tran, I. Aharonovich, D. Englund, *Optica* **2016**, *3*, 768.
- [34] M. Widmann, S. Y. Lee, T. Rendler, N. T. Son, H. Fedder, S. Paik, L. P. Yang, N. Zhao, S. Yang, I. Booker, A. Denisenko, M. Jamali, S. A. Momenzadeh, I. Gerhardt, T. Ohshima, A. Gali, E. Janzén, J. Wrachtrup, *Nat. Mater.* **2015**, *14*, 164.
- [35] D. M. Lukin, C. Dory, M. A. Guidry, K. Y. Yang, S. D. Mishra, R. Trivedi, M. Radulaski, S. Sun, D. Vercruysee, G. H. Ahn, J. Vučković, *Nat. Photonics* **2020**, *14*, 330.
- [36] A. L. Crook, C. P. Anderson, K. C. Miao, A. Bourassa, H. Lee, S. L. Bayliss, D. O. Bracher, X. Zhang, H. Abe, T. Ohshima, E. L. Hu, D. D. Awschalom, *Nano Lett.* **2020**, *20*, 3427.
- [37] F. Fuchs, B. Stender, M. Trupke, D. Simin, J. Pflaum, V. Dyakonov, G. V. Astakhov, *Nat. Commun.* **2015**, *6*, 7578.
- [38] N. H. Wan, T. J. Lu, K. C. Chen, M. P. Walsh, M. E. Trusheim, L. de Santis, E. A. Bersin, I. B. Harris, S. L. Mouradian, I. R. Christen, E. S. Bielejec, D. Englund, *Nature* **2020**, *583*, 226.
- [39] N. T. Son, C. P. Anderson, A. Bourassa, K. C. Miao, C. Babin, M. Widmann, M. Niethammer, J. Ul Hassan, N. Morioka, I. G. Ivanov, F. Kaiser, J. Wrachtrup, D. D. Awschalom, *Appl. Phys. Lett.* **2020**, *116*, 0004454.
- [40] D. M. Lukin, M. A. Guidry, J. Vučković, *PRX Quantum* **2020**, *1*, 020102.
- [41] A. Senichev, Z. O. Martin, S. Peana, D. Sychev, X. Xu, A. S. Lagutchev, A. Boltasseva, V. M. Shalae, *Sci. Adv.* **2021**, *7*, abj0627.
- [42] K. Ikeda, R. E. Saperstein, N. Alic, Y. Fainman, *Opt. Express* **2008**, *16*, 12987.
- [43] D. J. Moss, R. Morandotti, A. L. Gaeta, M. Lipson, *Nat. Photonics* **2013**, *7*, 597.
- [44] J. M. Arrazola, V. Bergholm, K. Brádler, T. R. Bromley, M. J. Collins, I. Dhand, A. Fumagalli, T. Gerrits, A. Goussev, L. G. Helt, J. Hundal, T. Isacsson, R. B. Israel, J. Izaac, S. Jahangiri, R. Janik, N. Killoran, S. P. Kumar, J. Lavoie, A. E. Lita, D. H. Mahler, M. Menotti, B. Morrison, S. W. Nam, L. Neuhaus, H. Y. Qi, N. Quesada, A. Repeating, K. K. Sabapathy, M. Schuld, et al., *Nature* **2021**, *591*, 54.
- [45] OIDA, *Optica Industry Report* **2021**, 24.
- [46] A. Senichev, S. Peana, Z. O. Martin, O. Yesilyurt, D. Sychev, A. S. Lagutchev, A. Boltasseva, V. M. Shalae, *ACS Photonics* **2022**, *9*, 3357.
- [47] S. Peana, O. Yesilyurt, A. Senichev, Z. O. Martin, V. Mkhitarian, A. S. Lagutchev, A. Boltasseva, V. M. Shalae, in *Frontiers in Optics + Laser Science 2022 (FIO, LS)*, Optica Publishing Group, Washington, DC **2022**.
- [48] M. A. Feldman, C. E. Marvinney, A. A. Poretzky, B. J. Lawrie, *Optica* **2021**, *8*, 1.
- [49] M. A. Feldman, A. Poretzky, L. Lindsay, E. Tucker, D. P. Briggs, P. G. Evans, R. F. Haglund, B. J. Lawrie, *Phys. Rev. B* **2019**, *99*, 020101.
- [50] A. Dietrich, M. W. Doherty, I. Aharonovich, A. Kubanek, *Phys. Rev. B* **2020**, *101*, 081401.
- [51] B. Sontheimer, M. Braun, N. Nikolay, N. Sadzak, I. Aharonovich, O. Benson, *Phys. Rev. B* **2017**, *96*, 121202.
- [52] K. M. C. Fu, C. Santori, P. E. Barclay, L. J. Rogers, N. B. Manson, R. G. Beausoleil, *Phys. Rev. Lett.* **2009**, *103*, 256404.
- [53] A. M. Berhane, K. Y. Jeong, Z. Bodrog, S. Fiedler, T. Schröder, N. V. Triviño, T. Palacios, A. Gali, M. Toth, D. Englund, I. Aharonovich, *Adv. Mater.* **2017**, *29*, 1605092.
- [54] S. Liu, Y. Shu, M. Zhu, H. Qin, X. Peng, *Nano Lett.* **2022**, *22*, 3011.
- [55] C. Clear, R. C. Schofield, K. D. Major, J. Iles-Smith, A. S. Clark, D. P. S. McCutcheon, *Phys. Rev. Lett.* **2020**, *124*, 153602.
- [56] B. C. Johnson, J. Woerle, D. Haasmann, C. T. K. Lew, R. A. Parker, H. Knowles, B. Pingault, M. Atature, A. Gali, S. Dimitrijević, M. Camarda, J. C. McCallum, *Phys. Rev. Appl.* **2019**, *12*, 044024.
- [57] J. Szépvölgyi, I. Mohai, *Ceram. Int.* **1999**, *25*, 711.
- [58] Y. Li, L. Wang, S. Yin, F. Yang, P. Wu, *J. Am. Ceram. Soc.* **2011**, *94*, 4169.
- [59] H. Schmidt, W. Gruber, G. Borchardt, M. Bruns, M. Rudolphi, H. Baumann, *Thin Solid Films* **2004**, *450*, 346.
- [60] H. Akbari, S. Biswas, P. Kumar Jha, J. Wong, B. Vest, H. A. Atwater, *Nano Lett.* **2022**, *22*, 7798.
- [61] V. M. Acosta, C. Santori, A. Faraon, Z. Huang, K.-M. C. Fu, A. Stacey, D. A. Simpson, K. Ganesan, S. Tomljenovic-Hanic, A. D. Greentree, S. Praver, R. G. Beausoleil, *Phys. Rev. Lett.* **2012**, *108*, 206401.
- [62] N. H. Wan, T. J. Lu, K. C. Chen, M. P. Walsh, M. E. Trusheim, L. De Santis, E. A. Bersin, I. B. Harris, S. L. Mouradian, I. R. Christen, E. S. Bielejec, D. Englund, *Nature* **2020**, *583*, 226.